Angiogenesis (2021) 24:489–504
https://doi.org/10.1007/s10456-020-09760-8

ORIGINAL PAPER

YAP promotes ocular neovascularization by modifying PFKFB3-driven endothelial glycolysis

Yifan Feng[1] · Rong Zou[1] · Xi Zhang[1] · Minqian Shen[1] · Xiuping Chen[1] · Jing Wang[1] · Weiran Niu[1] · Yuanzhi Yuan[1] · Fei Yuan[1]

Received: 22 June 2020 / Revised: 24 October 2020 / Accepted: 30 November 2020 / Published online: 5 January 2021
© The Author(s), under exclusive licence to Springer Nature B.V. part of Springer Nature 2021

Abstract

Ocular neovascularization is the leading cause of vision impairment in a variety of ocular diseases, such as age-related macular degeneration and retinopathy of prematurity. Emerging studies have suggested that the yes-associated protein (YAP), a downstream effector of the Hippo pathway, is involved in the pathological angiogenesis, but the mechanism are largely unknown. Here, we demonstrated that hypoxic treatment triggered YAP expression and nuclear translocation in human umbilical vein endothelial cells (HUVECs). YAP acted as a transcriptional co-activator working together with transcriptional enhancer activator domain 1 (TEAD1) to binds the promoter of the key glycolytic regulator 6-phosphofructo-2-kinase/fructose-2,6-biphosphatase3 (PFKFB3), and thereby increases PFKFB3 expression. Moreover, silencing of YAP inhibited glycolysis as well as proliferation, migration, sprouting and tube formation of HUVECs under hypoxia, all of which could be reversed by enforced expression of PFKFB3. Finally, our animal study also showed that intravitreal injection of small interfering RNA of YAP or PFKFB3 dramatically suppressed the neovascular growth in mouse models of choroidal neovascularization and oxygen-induced retinopathy. These findings provide new insights into a previously unrecognized effect of YAP on endothelial glycolysis and highlight the potential of targeting YAP/PFKFB3 axis in the treatment of ocular neovascularization.

Keywords Neovascularization · Endothelial cells · YAP · PFKFB3 · Glycolysis

Introduction

Ocular neovascular diseases, especially posterior segment neovascularization (NV) like immature retinopathy of prematurity (ROP), diabetic retinopathy (DR), and "wet" age-related macular degeneration (AMD), are the leading causes of vision impairment and irreversible blindness for individuals in developed and developing countries [1, 2]. This group of highly prevalent diseases is characterized by aberrant formation of immature blood vessels, which can result in hemorrhage, edema, retinal detachment and eventual blindness [3, 4]. Substantial evidence indicates that these eye diseases share molecular mechanisms because in each, sustained ischemia or hypoxia in retina or subretinal space [5], and hypoxia-induced imbalance between pro-angiogenic and anti-angiogenic molecules play an important role in the process of pathologic sprouting of new vessels [6, 7]. Endothelial cells (ECs) are especially critical in the process of NV. Increased endothelial activation, for instance, abnormal proliferation and migration in response to hypoxic-ischemic stimuli, are major cellular events causing new vessels sprouting [8]. However, the exact molecular mechanism underlying endothelial activation in ocular NV is still not fully clarified yet and further research is necessary to clarify it.

Metabolic aberrations in ECs have been confirmed to mediate the activity of ECs and contribute to the

Yifan Feng, Rong Zou, and Xi Zhang have contributed equally to this work.

Supplementary Information The online version of this article (https://doi.org/10.1007/s10456-020-09760-8) contains supplementary material, which is available to authorized users.

✉ Yuanzhi Yuan
yuan.yuanzhi@zs-hospital.sh.cn

✉ Fei Yuan
yuanfei_zs@126.com

[1] Department of Ophthalmology, Zhongshan Hospital, Fudan University, 180 # Fenglin Road, Shanghai 200032, China

development of pathological NV [9–11]. Compared with many other healthy cell types, ECs have much higher glycolytic activity and rely on glycolysis rather than oxidative metabolism for ATP production and vessel sprouting [12]. 6-phosphofructo-2-kinase/fructose-2,6-bisphosphatase isoform 3 (PFKFB3), the most abundant isoenzyme in various EC subtypes, produces the fructose-2,6-bisphosphate (F2,6P2), which allosterically activates the rate-limiting glycolytic enzyme phosphofructokinase-1 (PFK1). Several previous studies demonstrated that hypoxia or angiogenic factors [e.g., vascular endothelial growth factor (VEGF)] treatment upregulated the expression of endothelial PFKFB3 [13]; whereas reducing endothelial glycolysis by either pharmacological inhibition (with the small molecule 3PO) or genetic deletion of PFKFB3 could impair EC proliferation and migration in vitro and reduce pathological NV in vivo [13–15]. These data indicate a cell or tissue-context function of PFKFB3 in ocular NV progression.

Yes-associated protein (YAP) has been identified as the key downstream effector of the Hippo pathway, which serve important roles in regulation of tissue growth and organ morphogenesis, by modulating cell-cell contact, cell polarity, mechanical cues, secreted mitogens, and cellular metabolic status [16, 17]. In mammalian systems, the Hippo signaling pathway sequesters YAP to the cytoplasm via phosphorylating YAP at serine 127 (S127) [18]. When the Hippo pathway is inactive, the unphosphorylated YAP can translocate into the nucleus and bind to the TEAD family of transcription factors to activate target gene expression [19]. Accumulating evidence has proved that YAP is involved in both physiological and pathological NV, due to its critical role in migration, proliferation and junction assembly which are all required for the regulation of EC sprouting, vascular barrier formation and maturation [20, 21]. Interestingly, YAP recently has been described as a key metabolic hub in the regulation of glycolysis [22, 23]. For example, active YAP promoted glycolysis in tumor cells by elevating the expression of glucose-transporter 3 (GLUT3) [24] or Hexokinase 2 (HK2) [25]. Prompted by these observations, we wondered whether there is a potential connection between the YAP and the PFKFB3-mediated endothelial glycolysis during ocular NV development.

Here, we showed that YAP plays essential roles in PFPFB3 expression and glycolysis in human umbilical vein endothelial cells (HUVECs) under hypoxic conditions. Moreover, silence of YAP with small interfering RNA (siRNA) significantly inhibited the hypoxia-induced proliferation, migration and tube formation of HUVECs, which was partially reversed by PFKFB3 overexpression. Finally, using mouse models of laser-induced CNV and oxygen-induced retinopathy (OIR), we demonstrate that YAP/PFKFB3 axis is critically involved in pathological NV.

Materials and methods

Cell culture

Primary HUVECs were obtained from ScienCell Research Laboratories (Santiago, CA, USA) and used between passages 3–8. The type of cells and no pathogen (including mycoplasma) contamination were confirmed by the supplier. HUVECs were cultured in EC medium (ECM) with 5% fetal bovine serum (FBS), EC growth supplement (ECGS) and 1% penicillin/streptomycin at 37 °C in a modular incubator chamber (Thermo Scientific, Waltham, MA) containing 5% CO_2 under normoxic (21% O_2) or hypoxic (1% O_2 and 94% N_2) condition for 0–24 hours (h).

Cell transfection

The pcDNA3-Flag-YAP and pcDNA3-HA-TEAD1 plasmids were constructed by GenePharma (Shanghai, China). The siRNAs targeting YAP (siYAP), PFKFB3 (siPFKFB3) and the negative control (siCTRL) were obtained from RiboBio Co., Ltd (Guangzhou, China). Transfections of the HUVECs with plasmids or siNRAs (50 nM) were performed using a Lipofectamine® 2000 kit (Thermo Fisher Scientifc, Inc.), according to the manufacturer's protocols. Transfected HUVECs were incubated at 37 °C and 5% CO_2 in a humidified incubator for 36 h, and then collected for further experiment. The sequences of the siRNAs were present in Supplemental Table 1.

Virus infection

The non-mutated full-length YAP, 5SA and S94A-mutated YAP plasmids were purchased from Addgene (plasmid #33,091, #33,093 and #33,094) (Cambridge, MA), and subcloned into the MluI site of the retroviral vector pLNCX2. The recombinant lentivirus was packaged in 293T cells using standard methods. The adenovirus containing the full-length coding DNA sequence of PFKFB3 and the relative control were constructed by GenePharma (Shanghai, China). Cells were infected twice by retrovirus or adenovirus with the addition of Polybrene (8 μg/ml) and selected with puromycin (2 μg/ml).

Western blotting

Total protein was extracted from HUVECs or mouse retinal pigment epithelium (RPE)/choroid/sclera complexes using RIPA lysis buffer (Beyotime, Jiangsu, China), containing a protease inhibitor and phenylmethylsulfonyl fluoride. Following centrifugation of the lysates at 12,000×*g* for 15 min

at 4 °C, the supernatants were collected, and total protein was quantified using a BCA assay kit (Beyotime). Equal amounts of protein from each sample were separated by 10% SDS-PAGE and subsequently transferred onto polyvinylidene fluoride membranes (Millipore, Bedford, MA, USA). Membranes were blocked with 5% skimmed milk (Sigma-Aldrich; Merck KGaA) in TBS-0.05% Tween-20 (TBST) buffer (Sangon Biotech Co., Ltd.) at room temperature for 2 h and then incubated with the following primary antibodies (1:1000) at 4 °C overnight. Following the primary antibodies incubation, the membranes were reacted with the secondary antibody for 1 h. The reactive bands were detected and observed via an enhanced chemiluminescence (ECL) Kit. Densitometric quantifications of bands were done with Image J software (National Institutes of Health) using β-actin as an internal reference. Antibodies for western blot analysis are listed in Supplemental Table 2.

Real-time PCR

Total RNA from HUVECs was isolated using Trizol (Invitrogen, Carlsbad, CA, USA) and then reverse transcribed with PrimeScript RT Master mix (Takara, Otsu, Japan). Real-time PCR was conducted using an ABI PRISM 7500 fast real-time PCR System (Applied Biosystems, Foster City, CA, USA) with SYBR Premix Ex TaqTM II Kit (Takara) according to the manufacturer's instructions. The primer sequences used in this research are provided in Supplemental Table 3.

Reactive oxygen species (ROS) staining

The dihydroethidium (DHE) staining was used to detect ROS. HUVECs in different groups were fixed with 4% paraformaldehyde for 20 min, and then were incubated with 10 μmol/l of DHE (Beyotime) at 37 °C for 30 min, followed with 4′,6-diamidino-2-phenylindole (DAPI) for 3 min to visualize nuclear DNA. Images were then acquired by an inverted microscope (BX63; Olympus, Tokyo, Japan).

Immunofluorescent staining

HUVECs in different groups cultured on coverslips were fixed by 4% paraformaldehyde for 20 min and then extracted with 0.5% Triton X-100 solution for 5 minutes. After blocking with TBST containing 1% bovine serum albumin, cells were incubated with indicated primary antibodies anti-YAP1 (1:500, Abcam) and anti-PFKFB3 (1:100; Abcam) for 1 h. After that, cells were washed and incubated with fluorescein isothiocyanate or rhodamine-conjugated second primary antibodies (1:3000, Jackson ImmunoResearch) for 1 h, following with DAPI for 3 min. Images were captured with an inverted microscope (Olympus).

Glucose uptake and lactate release assays

The glucose uptake and lactate production in the culture supernatants were quantified using Glucose Uptake Fluorometric Assay Kit (#MAK084, Sigma-Aldrich) and Lactate Colorimetric/Fluorometric Assay Kit (#MAK064, Sigma-Aldrich) as per the manufacturer's recommendations. All the raw data were normalized by cell density measured by hemocytometer on a microscope.

Metabolic measurements

The Seahorse XFe 96 Extracellular Flux Analyzer (Seahorse Bioscience, MA, USA) was used to determine the extracellular acidification rate (ECAR) and oxygen consumption rate (OCR), according to the manufacturer's instructions. In brief, HUVECs (1×10^4 cells/well) were seeded into a Seahorse XF 96 cell culture plate and maintained in non-buffered assay medium in a non-CO_2 incubator for 1 h before the assay. For ECAR assay, glucose (10 mM), mitochondrial/ATP synthase inhibitor oligomycin (2 μM), and the glycolysis inhibitor 2-deoxyglucose (2-DG, 100 mM) were sequentially injected into each well at the time points specified. For OCR assay, mitochondrial respiration inhibitor, including oligomycin (2 μM), carbonylcyanide-4-trifluoromethoxyphenylhydrazone (FCCP, 1 μM) and rotenone/antimycin A (1.5 μM), was auto-injected into the experimental wells, followed by another three measurement cycles.

Chromatin immunoprecipitation (ChIP) assay

ChIP assay were conducted using the EZ-ChIP™ kit (Millipore). Briefly, protein-DNA complexes were cross-linked by 1% formaldehyde then quenched using 125 mM glycine. Cells were collected in shearing buffer (Diagenode, Denville, NJ, USA) and chromatin was sheared to an average DNA fragment size of 0.5-1 kb using a Bioruptor sonicator (Diagenode). After centrifugation, the supernatant was incubated with IgG or specific antibodies for TEAD1 and YAP, and chromatin DNA was purified and subjected to real-time PCR detection. The antibodies for immunoprecipitation and primers for the PFKFB3 promoter containing putative TEAD1 binding sites were present in Supplemental Tables 2 and 4.

Immunoprecipitation (IP) assay

For IP assay, cultured HUVECs cells were cotransfected with the pcDNA3-Flag-YAP and pcDNA3-HA-TEAD1 plasmids for 48 h and then lysed. For each IP sample, 500 μl of the lysate was incubated overnight at 4 °C with 10 μl of Protein G agarose beads (Thermo Fisher Scientific) and 1 μg of the indicated antibody on a rocking platform. Then,

beads-antibody complex was washed three times with cold IP buffer and boiled for 10 min to obtain protein supernatant captured by the protein G-sepharose beads. Finally, Immunoprecipitates were probed by western blotting with the indicated primary antibodies. Antibodies for western blot and IP analysis are listed in Supplemental Table 2.

Luciferase reporter gene assays

A total of 100 ng of pGL3-Basic plasmid (Promega Corporation, Madison, WI, USA) with inserts of the PFKFB3 promoter sequence (TSS: − 2000 ~ + 50) were co-transfected into HUVECs using Lipofectamine® 2000 transfection reagent (Thermo Fisher Scientifc) along with 200 ng of empty vector, YAP-5SA/TEAD1, or YAP-S94A/TEAD1 expression vectors and 10 ng of Renilla luciferase pRL-TK plasmid (Promega). After 48 h, the luciferase activity in the cells was measured with a Dual-Luciferase Reporter Assay system, according to the manufacturer's instructions (Promega). Relative luciferase activities were expressed as the ratio of firefly to Renilla luciferase activity.

Cell viability assay

The viability of HUVECs was evaluated by CCK-8 assay (Beyotime Institute of Biotechnology), according to the manufacturer's protocols. Briefly, HUVECs in different groups (1000 cells/well) were seeded into 96-well plates. At 24, 48 and 72 h, 10 μl CCK-8 reagent was added into each well, and the plates were incubated at 37 °C for additional 2 h. The absorbance was measured at 450 nm using a microplate spectrophotometer (Thermo Fisher Scientific Inc.).

Scratch wound assay

The migratory ability of HUVECs was analyzed using a wound healing assay. Briefly, when the monolayer of cells reached 100% confluence in 6-well plates, a 20-μl sterile pipette tip was used to create the wound. Cells were washed with 1 × PBS three times to remove the detached and damaged cells. Then, the cells were incubated in serum-free ECM under normoxic and hypoxic conditions. At 0 and 24 h incubation, the cells were imaged and the wound closure area was used to calculate the migratory ability of cells using Image J software.

Tube formation assay

The tube formation assay was conducted as previously described. Briefly, aliquots (150 μl) of Matrigel (BD Biosciences) were added to a 48-well plate and were incubated at 37 °C for 30 min. The cells were resuspended in supernatants collected from each pretreatment and then were seeded onto the gel (2×10^4 cells/well). Five random fields from each well were chosen and photographed after 8 h. Networks of tube-like structures were measured using Image J software.

Cell apoptosis assay

Terminal deoxynucleotidyl transferase dUTP nick end labeling (TUNEL) staining assay was used to quantify cell apoptosis. Briefly, the cells were fixed with 4% paraformaldehyde for 30 min at room temperature, washed two times with PBS, and permeabilized with 0.1% Triton X-100 for 5 min. Subsequently, the cells were subjected to TUNEL staining (Roche, Basel, Switzerland) for 1 h at room temperature in the dark, followed by 4′,6-diamidino-2-phenylindole (DAPI, Sigma-Aldrich, St. Louis, MO, USA) staining for the detection of cell nuclei. Images were acquired using a fluorescence microscope from three fields selected randomly in each well. The number of apoptotic cells was quantified using Image J software.

Animals and ocular NV models establishment

Pups and six to eight-week old male C57BL/6J mice were purchased from SLAC Laboratory Animal Co, Ltd (Shanghai, China). All animal protocols were approved by the Ethical Committee on Animal Experiments of Animal Care Committee of Fudan University. The animals were handled in accordance with the ARVO Statement for the Use of Animals in Ophthalmic and Vision Research. Animals were allowed to acclimatize for at least seven days before experimental manipulations.

CNV was induced by photocoagulation and was evaluated as previous described [26, 27]. In brief, mice were anaesthetized with 2% sodium pentobarbital (30 mg/kg, Sigma), and pupils of both eyes were dilated with 1% tropicamide (Alcon Laboratories, Inc, Fort Worth, TX, USA). Laser photocoagulation (532 nm wavelength, 120 mW power, 50 μm spot size, 100 ms duration) was performed bilaterally in each mouse. Four to six laser spots were applied around the optic nerve using a slit lamp delivery system and using a cover slip as a contact lens. The bubbling or pop sensing with laser photocoagulation was considered to be successful rupture of Bruch's membrane. Spots containing haemorrhage or failing to develop a bubble at the laser site were excluded from the analysis. Given the prolonged stability and good cell penetration of cholesterol-linked siRNAs [28, 29], cholesterol-modified YAP siRNA, PFKFB3 siRNA or scramble siRNA (Ribobio, Guangzhou, China) were injected intravitreally at 0.1 nmol in either eye of adult mice on day 1 (d1) after photocoagulation, according to established protocols [26]. Mice were killed at d7.

OIR model was induced as described before [25]. The pups and their foster/nursing mothers were placed in a high-oxygen chamber (75 ± 2% O_2) by post-natal day 7 (P7) for 5 days and then returned to room air (21% O_2) conditions. All siRNAs were injected intravitreally at 0.1 nmol in either eye of pups on P12 if needed. Pups were killed at P17.

Choroidal and retinal flatmount

Retinal fat mounts were performed on P7, P14 or P17 for retinal vascular development analysis, while choroidal fat mounts on d7 for CNV analysis, as described previously [30, 31]. In brief, after fixation with 4% paraformaldehyde and incubation with a blocking solution that contained 0.5% bovine serum albumin and 0.1% Triton X-100 in PBS, Retinal and RPE-choroid-sclera complex tissues were stained with FITC-conjugated Bandeiraea simplicifolia lectin isolectin B4 (IB4 lectin; 1:100; Sigma-Aldrich) and Alexa-Fluor 647-conjugated anti-PFKFB3 (1:1000; Abcam) in blocking buffer at 4 °C overnight. With 4–6 relaxing radial cuts, the retinal and RPE-choroid-sclera complex tissues were flat-mounted flat on a glass slide. All fat mounts were examined and photographed under a confocal laser scanning microscopy (FV3000, Olympus).

Aortic ring sprouting assay

Aortic ring assay was performed following previous protocol [32]. In brief, thoracic aortas were removed from adult mice, cleaned and transfected with siCTRL, siYAP with or without plasmid overexpressed PFKFB3 using Lipofectamine 2000 reagent (Invitrogen) overnight. The aortas were then embedded in 80 µl matrigel in a 96-well plate containing 500 µl opti-MEM Reduced Serum Media (Gibco) supplemented with 2.5% FBS. Endothelial sprouts were allowed to grow over 5 days with medium changing every other day. Quantification of vessel sprouting was performed by measuring the relative area of aortic explants outgrowth using image software (Image J, NIH).

Enzyme-linked immunosorbent (ELISA) assay

Conditioned media of HUVECs were collected and centrifuged at 4 °C and 3000×*g* for 15 min remove particulates and stored at − 80 °C. The concentrations of VEGF were measured by use of the ELISA kit (R&D Systems, Minneapolis, MN, USA) specific for the 165-amino acid form of human VEGF according to the manufacturer's protocols. The concentrations of VEGF were calculated from a standard curve.

Statistical analysis

Statistical analysis commercial software was used for statistical analysis (SPSS 21.0; SPSS, Chicago, IL, USA). Each experiment was repeated at least 3 times. Data are expressed as means 6 SEM. Comparisons between 2 groups were performed by using Student's t tests and comparisons among > 2 groups by using 1-way ANOVA followed by Bonferroni's or Dunnett's post hoc test. Values of $p < 0.05$ were considered statistically significant.

Results

Hypoxia trigers YAP activation and PFKFB3 expression in ECs

In order to study the potential crosstalk between the YAP and PFKFB3, we first examined the expressions of YAP and PFKFB3 in HUVECs cultured under hypoxic conditions at different times (1, 3, 6, 12 and 24 h). As shown in Fig. 1a, b, the protein level of HIF-1α, YAP and PFKFB3 significantly increased, while phosphorylated (S127)-YAP decreased in a time-dependent manner after hypoxic stimulation, as seen in Western blotting analysis and was quantitatively analyzed. Consistently, hypoxic treatment for 6 h increased the mRNA expression of HIF-1α, PFKFB3, YAP or its paralog transcriptional coactivator with PDZ-binding motif (TAZ; also known as WWTR1), and two canonical YAP transcription target genes (CTGF and CYR61) (Supplemental Fig. 1a). Additionally, the immunofluorescence assay also revealed that hypoxia triggered significant YAP nuclear translocation and PFKFB3 expression in the HUVECs (Fig. 1c, d). In contrast, the mRNA, phosphorylated and total protein levels of YAP upstream kinases LATS1 were significantly upregulated under exposure to hypoxic conditions (Supplemental Fig. 1b, c). The above results suggested hypoxia simultaneously induced YAP activation and PFKFB3 expression in HUVECs, which was in a Hippoindependent manner.

YAP1–TEAD1 interaction is crucial for PFKFB3 expression in ECs

To explore the potential regulatory relationships between the YAP and PFKFB3, HUVECs were firstly transfected with YAP or PRKFB3 siRNAs. RT-PCR and Western blotting assay showed that knockdown of YAP markedly suppressed the hypoxia-induced expression of PFKFB3, whereas PFKFB3 silence had no significant effect on YAP expression in HUVECs, indicating that PFKFB3 was a potential downstream target gene of YAP signaling (Fig. 2a, b; Supplemental Fig. 2a). Next, we examined the role of activated YAP on PFKFB3 expression in HUVECs under normoxic

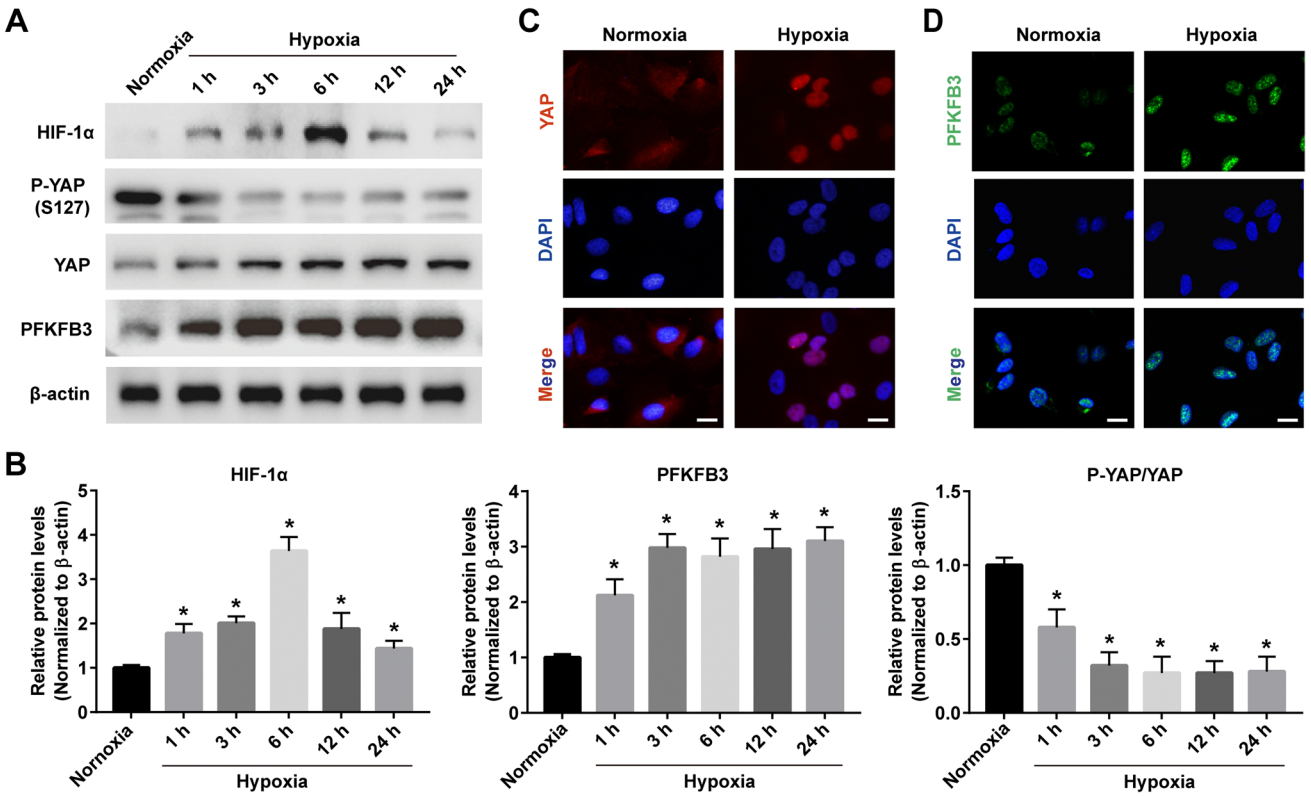

Fig. 1 Hypoxia triggers YAP activation and PFKFB3 expression in HUVECs. **a** Western blot analysis of HIF-1α, p-YAP (Ser127), YAP and PFKFB3 protein expression in HUVECs exposed to hypoxia (1% O_2) for indicated times. **b** Quantitative analysis for immunoblotting. ($n=4$ independent experiments/group). *$p<0.05$ vs. control cells under normoxia. **c** Immunostaining of YAP (red) and PFKFB3 (green) in HUVECs exposed to hypoxia (1% O_2) for 6 h. Nuclei were visualized by Dapi (blue). Scale bar = 50 μm

conditions. Using lentiviral infection, we established stably transduced HUVECs that overexpress full-length YAP, YAP-5SA (constitutively active YAP that cannot be phosphorylated by LATS kinases), YAP-S94A (TEAD-binding deficient YAP protein) and YAP-5SA-S94A. A higher level of PFKFB3 mRNA as well as protein was detected in full-length YAP and YAP-5SA cells than in vector-control cells, YAP-S94A cells or YAP-5SA-S94A cells by RT-PCR and Western blotting assay (Supplemental Fig. 2b, c). Similar findings were verified by the immunofluorescence analysis (Fig. 2c), suggesting that YAP transcriptional activity is required for PFKFB3 expression in HUVECs under normoxia or hypoxia.

Because TEAD1 is a primary mediator of YAP-dependent gene regulation in ECs [33, 34], we speculated that YAP regulated PFKFB3 at transcription level via binding with TEAD1. In order to confirm the existence of the YAP–TEAD1 complex, IP assays were performed and showed a direct interaction between YAP and TEAD1 (Fig. 2d). Using JASPAR (http://jaspar.genereg.net/) and Eukaryotic Promoter Database EPD (http://epd.vital-it.ch), we found two putative TEAD1 binding sites within the promoter region (3.0 KB) of PFKFB3 (Fig. 2e). Moreover, to determine whether YAP–TEAD1 complex regulates transcription of PFKFB3 directly, we carried out the ChIP assay. When precipitated with anti-TEAD1 or anti-YAP antibody, we detected positive PCR products at the P2 site relative to TSS of the proximal promoter regions of PFKFB3 (Fig. 2f). In addition, transfected with YAP-5SA-S941 or mutation of TEAD1-binding sites in the PFKFB3 promoter significantly attenuated YAP-5SA/TEAD1-induced PFKFB3 promoter luciferase activity (Fig. 2g), demonstrating that PFKFB3 is a direct transcriptional target of YAP. Taken together, these data indicated that YAP–TEAD1 complexes bound to PFKFB3 gene promoter and directly activated its transcription in hypoxia.

YAP/PFKFB3 axis controls hypoxia-induced EC glycolysis

Given the roles of YAP in promoting PFKFB3 transcription, we next examined whether YAP regulated EC glycolysis under hypoxic conditions. To confirm this, PFKFB3 overexpression plasmid were cotransfected into siYAP-treated HUVECs and we observed that such plasmid could almost reverse PFKFB3 levels (Fig. 3a, b). Hypoxia stimulation

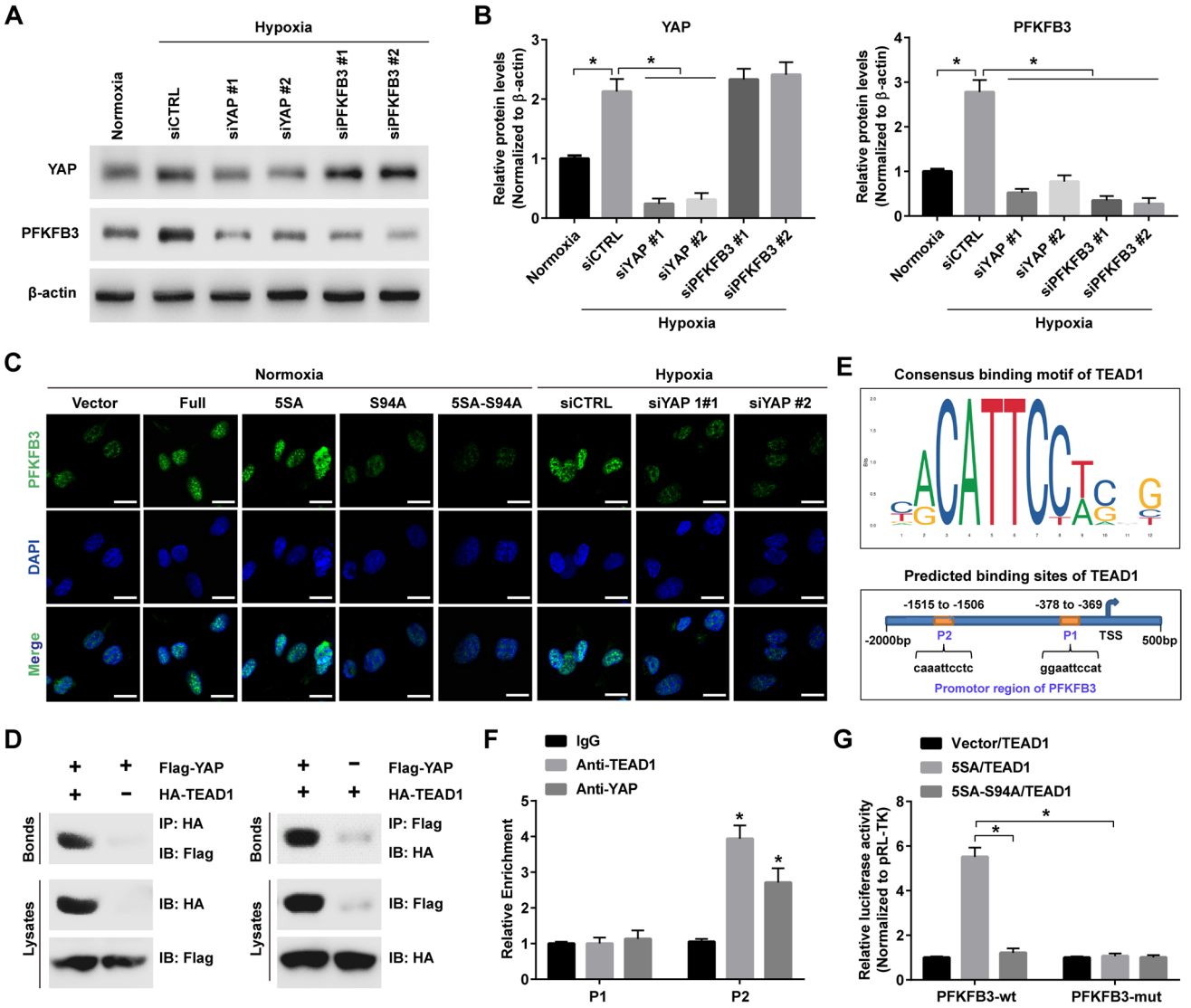

Fig. 2 YAP1–TEAD1 complexes are crucial for PFKFB3 expression in HUVECs. **a** Western blot analysis of protein levels of YAP and PFKFB3 in HUVECs transfected with siCTRL, siYAP #1 or #2, PFKFB3 #1 or #2 under hypoxia (1% O_2). HUVECs in normoxic group were cultured under normoxia (21% O_2). **b** Quantitative analysis for immunoblotting. ($n = 4$ independent experiments/group). *$p < 0.05$. **c** PFKFB3 protein expression levels were detected by immunostaining in HUVECs following retroviral delivery of empty vector, full-length YAP, YAP-5SA, YAP-S94A and YAP-5SA-S94A under normoxia (21% O_2, left panel) or in HUVECs transfected with siCTRL or siYAP #1 or #2 under hypoxia (1% O_2, right panel). Scale bar = 50 μm. **d** A co-immunoprecipitation assay was performed respectively to examine the interaction of YAP with TEAD1 in HUVECs transfected with the plasmids as indicated. **e** Consensus binding motif of TEAD1 and the binding sites of TEAD1 on the promoter of PFKFB3 were predicted using JASPAR database. **f** ChIP-qPCR analysis was used to confirm the enrichment of PFKFB3 at the different binding sites predicted using an YAP antibody or an TEAD1 antibody or a negative (IgG) antibody in HUVECs. ($n = 4$ independent experiments/group). *$p < 0.05$ versus IgG. **g** PFKFB3 promoter luciferase reporter assay was performed by overexpressing YAP-5SA or YAP-5SA-S94A, and TEAD1 in HUVECs ($n = 4$ independent experiments/group). *$p < 0.05$

led to an increase in the rate of glucose uptake and lactate release in HUVECs, while YAP knockdown strikingly inhibited hypoxia-induced glucose uptake and lactate production (Fig. 3c, d). ECAR (a measurement of lactate production and glycolysis) kinetic profiles further demonstrated that intracellular metabolites of glycolysis (pyruvate, lactate, and 3-phosphoglycerate) were markedly decreased in siYAP-treated cells when comparing with siCTRL-treated cells (Fig. 3e, f), further confirming that YAP is essential for EC glycolysis under hypoxic conditions. As expected, overexpression of PFKFB3 partly reversed the effects of YAP deletion on glycolysis (Fig. 3c–f). Furthermore, HUVECs exposing to hypoxia exhibited lower maximum respiratory capacity and higher ROS level than that cells cultured in

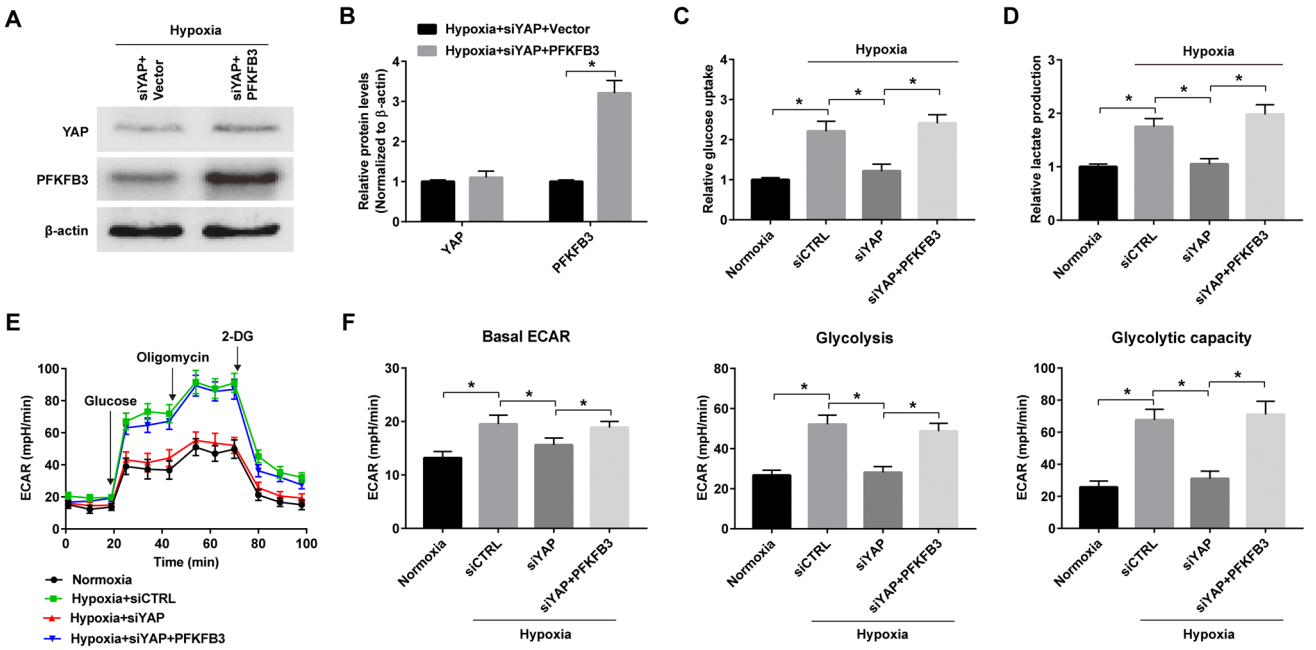

Fig. 3 YAP/PFKFB3 axis controls hypoxia-induced glycolysis in HUVECs. **a** Western blot analysis of YAP and PFKFB3 protein expression in HUVECs, which treated with siYAP and vector or PFKFB3 adenoviruses under hypoxia (1% O_2) for 6 h. **b** Quantitative analysis for immunoblotting. ($n = 4$ independent experiments/group). *$p < 0.05$. **c, d** Relative glucose uptake (**c**) and lactate production (**d**) in HUVECs under normoxia (21% O_2), or HUVECs treated with siCTRL, siYAP or siYAP in combination with PFKFB3 adenoviruses under hypoxia (1% O_2) for 6 h. ($n = 5$ independent experiments/group). *$p < 0.05$ vs. control cells under normoxia. **e** Extracellular acidification rate (ECAR) was measured by the sequential injection of glucose (10 mM), oligomycin (2 μM), and 2-DG (100 mM). **f** Quantification of glycolytic function parameters of (**e**). ($n = 4$ independent experiments/group). *$p < 0.05$

normoxia. However, YAP silencing alone or together with PFKFB3 over-expression had no effect on the maximum respiration rate (Supplemental Fig. 3a, b) and ROS levels (Supplemental Fig. 3c) in HUVECs under hypoxia. These data suggest that YAP/PFKFB3 axis is involved in hypoxia-induced glycolysis, but not oxidative phosphorylation and oxidative stress.

YAP/PFKFB3 axis controls hypoxia-induced VEGFA and VEGFR1 expression in ECs

It is widely acknowledged that VEGF is an important angiogenic factor that stimulates the formation of new blood vessels [35]. Our group and others have previously shown that hypoxia increased VEGF secretion and VEGF receptors expression in ECs [36–38]. Therefore, we also questioned whether YAP/PFKFB3 pathway has a substantial role in expressions of VEGF and its receptors VEGFR1 and VEGFR2. Western blot showed that the VEGFA and VEGFR1 protein levels displayed a steady rise during hypoxia compared to normoxia. In contrast, VEGFR2 protein levels were increased and reach a maximum at 12 h and then decreased at 24 h in hypoxia (Fig. 4a, b). In addition, to fully evaluate the expression of VEGFA, we also performed the ELISA method to quantify VEGFA released into the culture supernatant of HUVECs, and as shown in Fig. 4c, the concentrations of VEGFA in the culture cells were significantly increased under hypoxic conditions. Interestingly, YAP silencing decreased the hypoxia-induced secretion or expression of VEGFA and VEGFR1, and this effect was attenuated by PFKFB3 co-administration. However, knockdown of YAP has no effect on the VEGFR2 expression (Fig. 4d–f), which is consistent with previous finding that YAP silencing mainly impaired VEGFR2 cellular distribution and trafficking [39].

YAP/PFKFB3 axis regulates the biological function of ECs under hypoxia

In order to verify whether the YAP/PFKFB3 axis contributes to the biological response of ECs to hypoxia, CCK8 assays were employed and the results showed that hypoxic treatment inhibited cell proliferation (Fig. 5a), which was further aggravated by YAP knockdown. Conversely, YAP knockdown suppressed hypoxia-accelerated migration (Fig. 5b, c) and tube formation (Fig. 5d, f) of HUVECs. Moreover, we assessed the effect of YAP knockdown on endothelial cell sprouting by aortic sprouting assay, which showed that YAP knockdown attenuated sprouting in murine aorta cultured in hypoxia (Fig. 5e, g). In particular, co-transfection with

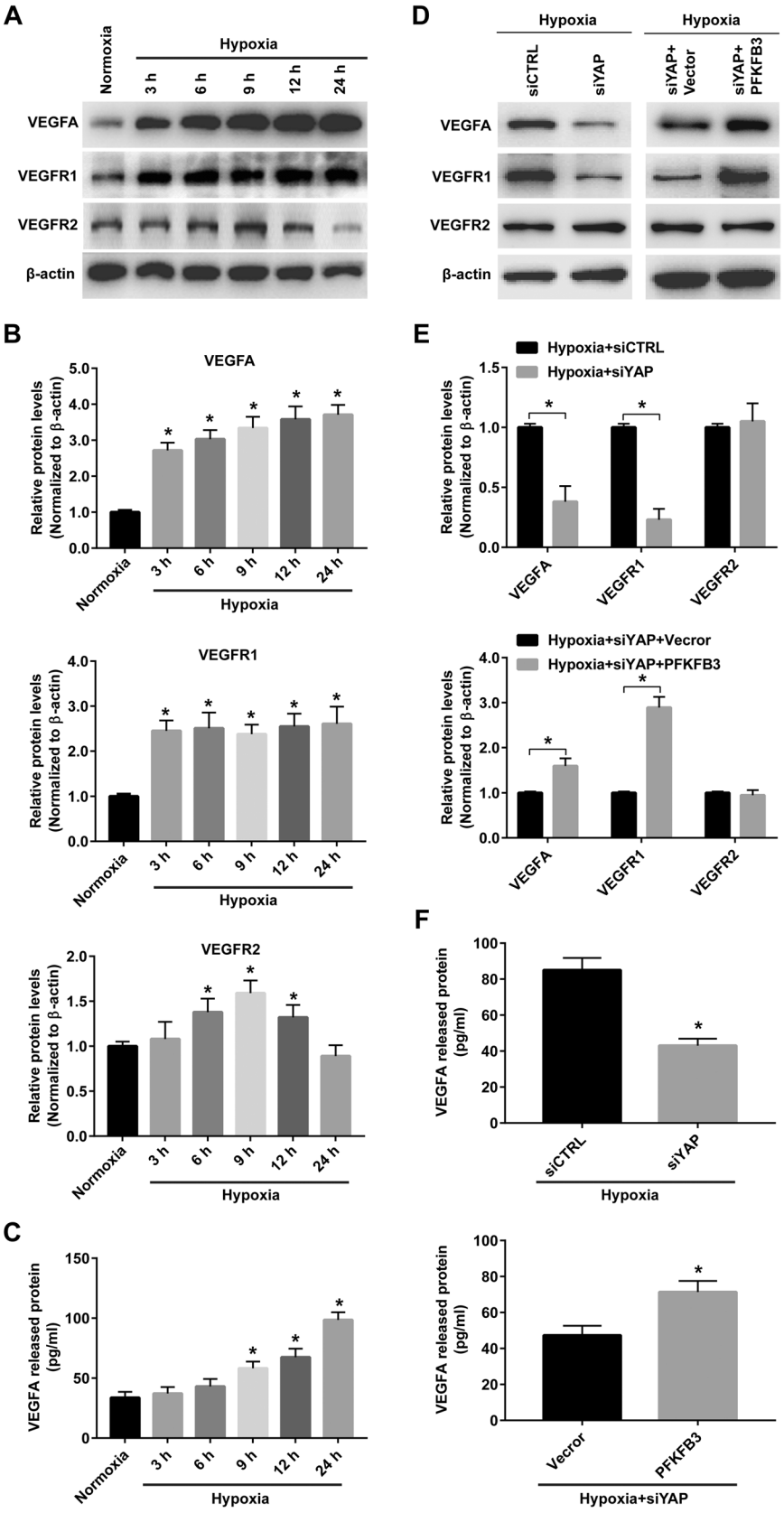

Fig. 4 YAP/PFKFB3 axis controls hypoxia-induced VEGFA and VEGFR1 expression in HUVECs. **a** Western blot analysis of VEGFA, VEGFR1 and VEGFR2 protein expression in HUVECs exposed to hypoxia (1% O_2) for indicated times. **b** Quantitative analysis for immunoblotting of (**a**). ($n = 4$ independent experiments/group). $^*p < 0.05$ vs. control cells under normoxia. **c** ELISA data shows the concentrations of VEGF released in the supernatant of HUVECs exposed to hypoxia (1% O_2) for indicated times. ($n = 3$ independent experiments/group). **d** Western blot analysis of VEGFA, VEGFR1 and VEGFR2 protein expression in HUVECs which treated with siCTRL, siYAP, siYAP plus the vector or PFKFB3 adenoviruses under hypoxia (1% O_2) for 9 h. **e** Quantitative analysis for immunoblotting of **d**. ($n = 4$ independent experiments/group). **f** ELISA data shows the concentration of VEGF released in the supernatant of HUVECs which treated with siCTRL, siYAP, siYAP plus the vector or PFKFB3 adenoviruses under hypoxia (1% O_2) for 24 h. ($n = 3$ independent experiments/group). $^*p < 0.05$

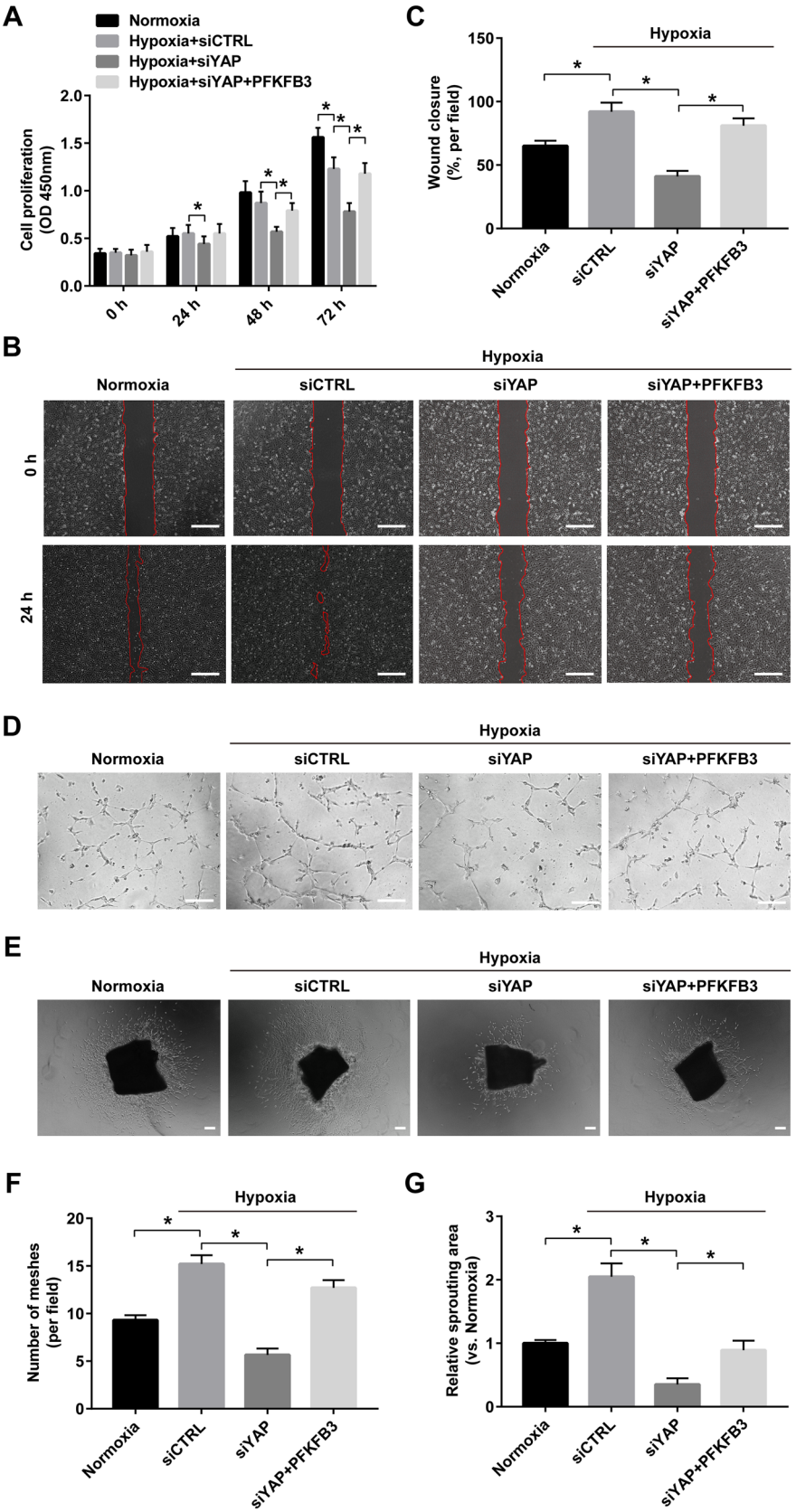
A
Normoxia
Hypoxia+siCTRL
Hypoxia+siYAP
Hypoxia+siYAP+PFKFB3
Cell proliferation (OD 450nm)
0 h
24 h
48 h
72 h
C
Hypoxia
Wound closure (%, per field)
Normoxia
siCTRL
siYAP
siYAP+PFKFB3
B
Hypoxia
Normoxia
siCTRL
siYAP
siYAP+PFKFB3
0 h
24 h
D
Hypoxia
Normoxia
siCTRL
siYAP
siYAP+PFKFB3
E
Hypoxia
Normoxia
siCTRL
siYAP
siYAP+PFKFB3
F
Hypoxia
Number of meshes (per field)
Normoxia
siCTRL
siYAP
siYAP+PFKFB3
G
Hypoxia
Relative sprouting area (vs. Normoxia)
Normoxia
siCTRL
siYAP
siYAP+PFKFB3

◂**Fig. 5** YAP/PFKFB3 axis regulates the biological function of HUVECs under hypoxia. **a** The proliferation of HUVECs was detected by CCK8 assay. HUVECs treated with siCTRL, siYAP or siYAP in combination with PFKFB3 adenoviruses for 36 h and then exposed to under hypoxia (1% O_2) for 24, 48 and 72 h. HUVECs in normoxic group were cultured under normoxia (21% O_2) for same time-points. ($n = 5$ independent experiments/group). $^*p < 0.05$. **b** Migration of HUVECs was assessed using a scratch wound assay. HUVECs treated with siCTRL, siYAP or siYAP in combination with PFKFB3 adenoviruses for 36 h were wounded with a p20 pipette tip and then exposed to under hypoxia (1% O_2) for 24 h. Photographs were taken immediately and after 24 h. HUVECs in normoxic group were cultured under normoxia (21% O_2) for same time-points. Scale bar = 500 μm. **c** The percent of closure areas were quantified and analyzed ($n = 4$ for wound assay and 3 fields were calculated per sample). $^*p < 0.05$. **d** Tube formation of HUVECs was assessed using a Matrigel assay. HUVECs treated with siCTRL, siYAP or siYAP in combination with PFKFB3 adenoviruses for 36 h and inoculated on GFR Matrigel surface under hypoxia for 6 h. HUVECs in normoxic group were cultured under normoxia (21% O_2) for same time-points. Scale bar = 500 μm. **e** Aortic rings isolated from adult mice were transfected with siCTRL, siYAP or siYAP in combination with PFKFB3 adenoviruses for overnight and cultured for 4 days. Aortic rings in normoxic group were cultured under normoxia (21% O_2) for same time-points. Scale bar = 200 μm. **f** The number of meshes formed was quantified and analyzed ($n = 4$ for Matrigel assay and 5 fields were calculated per sample). $^*p < 0.05$. **g** The sprouting areas were was quantified and analyzed. (4 independent experiments/group). $^*p < 0.05$

siYAP and PFKFB3 overexpressed plasmid could reverse the effects of siYAP on HUVEC proliferation, migration, sprouting and tube formation (Fig. 5a–g). Notably, TUNEL staining analyses revealed no differences in the number of apoptotic cells among the groups exposed to hypoxia, and all of which displayed increased number of apoptotic cells compared to the normoxic group (Supplemental Fig. 4).

Inhibition of either YAP or PFKFB3 ameliorates ocular neovascularization

At last, we assessed the effect of YAP and PFKFB3 on ocular neovascularization by intravitreal injection in vivo. We injected YAP, siPFKFB3 or scramble siRNAs intravitreally 1 day after laser coagulation in adult CNV model mice and collected choroidal tissues at d7 (Fig. 6a). Compared with the scramble group, mice treated with either YAP siRNA or PFKFB3 siRNA showed a marked decrease in CNV area as well as the PFKFB3 expression in areas of new vessels (Fig. 6b). Western blotting analysis showed that the protein levels of PFKFB3, VEGFA and VEGFR1 were observably reduced in choroidal tissues treated with YAP siRNA or PFKFB3 siRNA, compared to those treated with scramble siRNA (Fig. 6c, d). The same inhibitory effect was also observed in the retinal tissues of OIR model (Fig. 6g–i), as siRNAs was injected at P12 and retinal tissues were analyzed at P17 (Fig. 6f). Consequently, YAP or PFKFB3 knockdown could suppress pathological ocular neovascularization in vivo, therefore indicating their potential as novel therapeutic targets.

Discussion

Ocular NV is a complex, multistep process, which occurs in proximity to the areas that are most prone to the development of ischemia and hypoxia in cases of decreased blood flow [40, 41]. HUVECs exhibit similar endothelial phenotypes and functions to choroidal or retinal ECs, and therefore are widely used as main cell model for in vitro research of ocular angiogenesis [42, 43]. In this study, we demonstrated that hypoxia promotes YAP expression and nuclear translocation in HUVECs. Moreover, YAP acted as a transcriptional co-activator working together with TEAD1 to binds the PFKFB3 promoter and thereby increases PFKFB3 expression. Silencing of YAP inhibits hypoxia-enhanced endothelial glycolysis (e.g., glucose uptake and lactate production) and activation (e.g., proliferation, migration, sprouting and VEGFA/VEGFR1 expression), all which are reversed by PFKFB3 overexpression. Furthermore, our animal study also shows that intravitreal injection of YAP or PFKFB3 siRNA dramatically suppressed the neovascular growth in mouse models of OIR and CNV. These findings provide new insights into a previously unrecognized effect of YAP on endothelial glycolysis and highlight the potential of targeting YAP/PFKFB3 axis in the treatment of ocular NV (Fig. 7).

Previous studies showed that YAP is necessary for the vascular development of the retina [20, 39, 44]. YAP controls the proliferation and migration of ECs that regulate angiogenic sprouting and branching via activation of Myc signaling [20] and small GTPase CDC42 [20, 21], respectively. A recent study indicated that YAP interacted with signal transducer and activator of transcription factor 3 (STAT3) to promote STAT3 nuclear translocation and VEGF transcription, which boosted the hypoxia-induced proliferation, migration and tube formation of ECs [45]. In the same study, inhibition of YAP alleviated retinal pathological NV in mouse OIR model [45]. A high level of YAP was also detected in the vascular endothelium within laser-induced CNV lesion, which facilitates CNV formation via promoting endothelial cell proliferation [46]. Consistent with these results, our findings also further confirmed

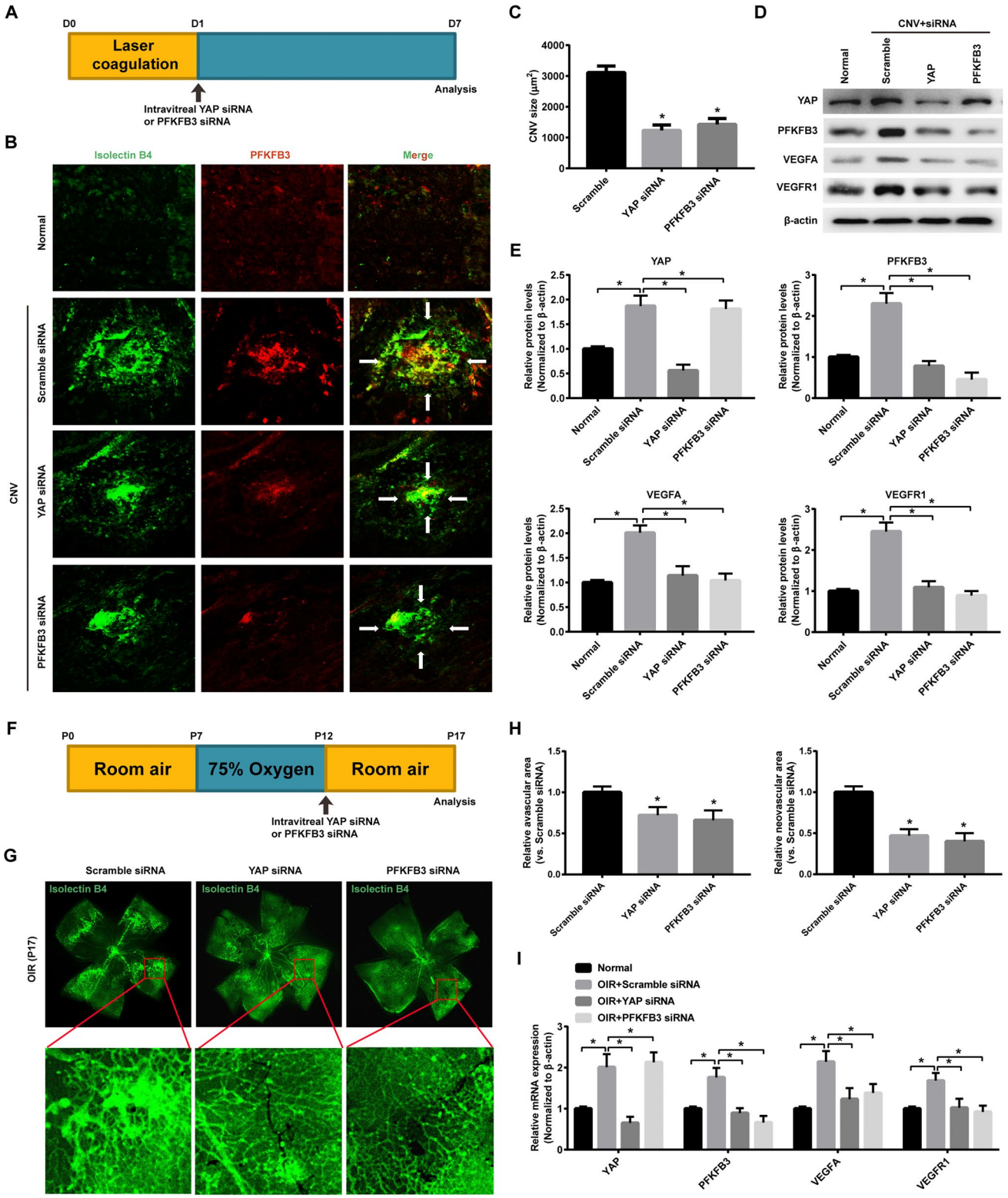
A
D0
D1
D7
Laser coagulation
Analysis
Intravitreal YAP siRNA or PFKFB3 siRNA
B
Isolectin B4
PFKFB3
Merge
Normal
CNV
Scramble siRNA
YAP siRNA
PFKFB3 siRNA
C
CNV size (μm²)
Scramble
YAP siRNA
PFKFB3 siRNA
D
CNV+siRNA
Normal
Scramble
YAP
PFKFB3
YAP
PFKFB3
VEGFA
VEGFR1
β-actin
E
YAP
PFKFB3
VEGFA
VEGFR1
Relative protein levels (Normalized to β-actin)
Normal
Scramble siRNA
YAP siRNA
PFKFB3 siRNA
F
P0
P7
P12
P17
Room air
75% Oxygen
Room air
Analysis
Intravitreal YAP siRNA or PFKFB3 siRNA
G
Scramble siRNA
YAP siRNA
PFKFB3 siRNA
Isolectin B4
OIR (P17)
H
Relative avascular area (vs. Scramble siRNA)
Relative neovascular area (vs. Scramble siRNA)
I
Normal
OIR+Scramble siRNA
OIR+YAP siRNA
OIR+PFKFB3 siRNA
Relative mRNA expression (Normalized to β-actin)
YAP
PFKFB3
VEGFA
VEGFR1

◂**Fig. 6** Inhibition of either YAP or PFKFB3 ameliorates ocular neovascularization. **a** Schematic diagram of intravitreal injection strategy in mouse CNV model. Mice received intravitreal injection of scramble, YAP or PFKFB3 siRNAs at d1 after laser coagulation and were killed at d7 for CNV analysis. **b, c** Whole choroidal tissues were flat mounted and stained with isolectin B4 (green) at d7 after photocoagulation and examined under a laser scanning confocal microscope. Representative images are shown in **b**, and quantitative of lesion size (square micrometers) is shown in **c** ($n = 5$–6/group; representative of 3 independent experiments). $^*p < 0.05$ vs. scramble siRNA group. **d** Western blot analysis of YAP, PFKFB3, VEGFA and VEGFR1 protein expression levels in choroidal tissues from normal or CNV-subjected mice at d7 after photocoagulation. **e** Quantitative analysis for immunoblotting. ($n = 8$–10/group; representative of 3 independent experiments). $^*p < 0.05$. **f** Schematic diagram of intravitreal injection strategy in mouse OIR model. Mice received intravitreal injection of scramble, YAP or PFKFB3 siRNAs at P12 after 75% oxygen uptake and were killed at P17 for OIR analysis. **g, h** Whole retinal tissues were flat mounted and stained with isolectin B4 (green) at P17 and examined under a laser scanning confocal microscope. Representative images are shown in **g**, and quantitative of neovascular and avascular area is shown in **h**. ($n = 8$–10/group; representative of 3 independent experiments). $^*p < 0.05$ vs. scramble siRNA group. **i** Real-time PCR analysis of YAP, PFKFB3, VEGFA and VEGFR1 mRNA expression levels in retinal tissues from normal or OIR-subjected mice at P17. ($n = 10$–12/group; representative of 3 independent experiments). $^*p < 0.05$

the proangiogenic role of YAP in hypoxia-mediated NV. Importantly, we have found that under hypoxic condition, knockdown of YAP led to a dramatic reduction of glycolysis in ECs that exhibit decreased glucose uptake and lactate production, suggesting that YAP is essential for hypoxia-triggered glycolysis in ECs.

ECs are mostly quiescent but can sense and respond to signals released from surrounding hypoxic tissue, resulting in a shift to highly glycolytic metabolism [11, 12]. Additionally, growth factors such as VEGF [15] and FGF2 [47] enhance the expression of glycolytic enzymes and increase glycolysis to support the high ATP demands for vessel sprouting, indicating that glycolysis is also critical for growth factor-driven angiogenesis. A recent study indicates that YAP promotes cell proliferation and glycolysis by upregulating GLUT3 expression in transformed cell lines [24]. PFKFB3 is a master glycolytic regulator in ECs, and pharmacological blockade or knockdown of PFKFB3 suppresses retinal neovascularization in mouse models of OIR and AMD [13, 15]. Therefore, we focus the regulated role of YAP on PFKFB3. Intriguingly, we showed here that the expression of PFKFB3 was decreased in YAP-silenced ECs, and ectopic expression of PFKFB3 partly reversed the suppressive effect of YAP silencing on glycolysis as well as proliferation, migration and tube formation of ECs, implying that loss of YAP may induce endothelial metabolic dysfunction by reducing PFKFB3-mediated glycolysis.

The decreased p-YAP expression and increased nuclear translocation of YAP under hypoxia is consistent with the results of Zhu et al. [45]. It has been reported that PFKFB3 is a hypoxia-inducible gene because its promoter contains HIF-1α binding sites [48, 49], However, our data provide evidence that nuclear transcription of YAP is crucial for PFKFB3 expression under mormoxic or hypoxic conditions. Given that YAP is a transcriptional co-activator and has no DNA-binding domains, we speculate that in addition to TEAD1 mediates transcriptional activity, YAP can also coactivate with HIF-1α to augment transcription of PFKFB3 gene under hypoxia. This hypothesis is supported by recent studies which showed that nuclear YAP serves as a "stress sensor" that cooperates with HIF-1α to drive pyruvate kinase M2 (PKM2) and govern tumor progression under hypoxic microenvironment [50–52]. Further detailed study is required to ascertain whether the hypoxia triggers formation of three distinct complexes or a ternary complex consisting of YAP–TEAD1–HIF-1α with all their properties.

VEGF plays an important role in the pathogenesis of ocular NV and anti-VEGF therapy has become an attractive clinical strategy in the treatment of these diseases [53, 54]. VEGF is synthesized by multiple populations within human retina, including endothelial cells, pericytes, neurons, and the retinal pigment epithelium [55], and increased secretion of VEGF in response to hypoxia occurs in these ocular cells [56]. In current study, we found that YAP knockdown led to a marked reduction in VEGFA and VEGFR1 expression, but not VEGFR2 in HUVECs under hypoxia, suggesting a facilitating role of YAP in the VEGF pathway. Unsurprisingly, ectopic expression of PFKFB3 could restore these genes. Although the mechanism is still unknown, the increased lactate levels upon PFKFB3 overexpression may contribute to the upregulation of VEGFA and VEGFR1 [57].

In summary, we have demonstrated that YAP–TEAD1 signaling makes an essential contribution to controlling endothelial function and angiogenesis under hypoxic conditions. We also found that YAP deletion dramatically impairs the endothelial behavior and pathological NV through the inhibition of PFKFB3-driven glycolysis. Manipulation of YAP–TEAD1–PFKFB3 pathway may potentially lead to the development of new therapeutic strategies for NV-related ophthalmic diseases.

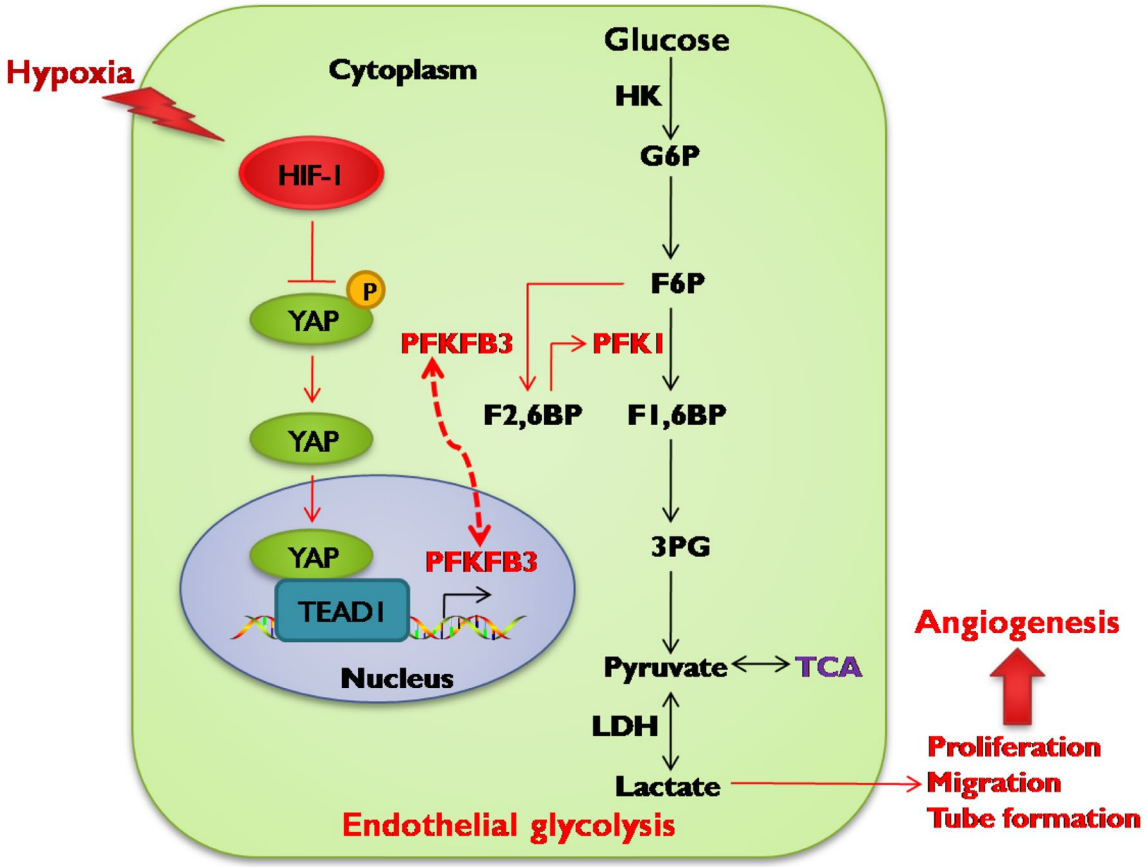

Fig. 7 Graphical abstract showing that the YAP regulates hypoxia-accelerated endothelial glycolysis and angiogenesis by affecting PFKFB3 transcription

Acknowledgements We would like to thank Dr. Jinhai Huang for technical assistance in ELISA and confocal imaging of the manuscript.

Author contributions YFF and FY designed the research; YFF, RZ, XZ, MQS and XPC performed the research; YFF, RZ and WRN analyzed the data; YFF and RZ wrote the paper; and YZY and FY revised manuscript.

Funding This study was supported by grants from the National Nature Science Foundation of China (No. 81970817, 81873680, 81800843 and 81600735) and the Excellent Youth Talent Program of Zhongshan Hospital (2017ZSYXQN30).

Compliance with ethical standards

Conflict of interest The authors declare that they have no confict of interest.

Ethical approval This article does not contain any studies with human participant performed by any of the authors. All animal protocols were approved by the Ethical Committee on Animal Experiments of Animal Care Committee of Fudan University (Permit Number: 2018-038).

References

1. Campochiaro PA (2013) Ocular neovascularization. J Mol Med (Berl) 91:311–321
2. Zhang SX, Ma JX (2007) Ocular neovascularization: Implication of endogenous angiogenic inhibitors and potential therapy. Prog Retin Eye Res 26:1–37
3. Selvam S, Kumar T, Fruttiger M (2018) Retinal vasculature development in health and disease. Prog Retin Eye Res 63:1–19
4. Afzal A, Shaw LC, Ljubimov AV et al (2007) Retinal and choroidal microangiopathies: therapeutic opportunities. Microvasc Res 74:131–144
5. Vadlapatla RK, Vadlapudi AD, Mitra AK (2013) Hypoxia-inducible factor-1 (HIF-1): a potential target for intervention in ocular neovascular diseases. Curr Drug Targets 14:919–935
6. Campochiaro PA (2015) Molecular pathogenesis of retinal and choroidal vascular diseases. Prog Retin Eye Res 49:67–81
7. Tolentino MJ (2009) Current molecular understanding and future treatment strategies for pathologic ocular neovascularization. Curr Mol Med 9:973–981
8. Carmeliet P, Jain RK (2011) Molecular mechanisms and clinical applications of angiogenesis. Nature 473:298–307
9. Li X, Sun X, Carmeliet P (2019) Hallmarks of endothelial cell metabolism in health and disease. Cell Metab 30:414–433

10. Rohlenova K, Veys K, Miranda-Santos I et al (2018) Endothelial cell metabolism in health and disease. Trends Cell Biol 28:224–236
11. Wong BW, Marsch E, Treps L et al (2017) Endothelial cell metabolism in health and disease: impact of hypoxia. EMBO J 36:2187–2203
12. Eelen G, de Zeeuw P, Treps L et al (2018) Endothelial cell metabolism. Physiol Rev 98:3–58
13. Xu Y, An X, Guo X et al (2014) Endothelial PFKFB3 plays a critical role in angiogenesis. Arterioscler Thromb Vasc Biol 34:1231–1239
14. Schoors S, De Bock K, Cantelmo AR et al (2014) Partial and transient reduction of glycolysis by PFKFB3 blockade reduces pathological angiogenesis. Cell Metab 19:37–48
15. De Bock K, Georgiadou M, Schoors S et al (2013) Role of PFKFB3-driven glycolysis in vessel sprouting. Cell 154:651–663
16. Zheng Y, Pan D (2019) The hippo signaling pathway in development and disease. Dev Cell 50:264–282
17. Huang J, Wu S, Barrera J et al (2005) The Hippo signaling pathway coordinately regulates cell proliferation and apoptosis by inactivating Yorkie, the Drosophila Homolog of YAP. Cell 122:421–434
18. Zou R, Xu Y, Feng Y et al (2020) YAP nuclear-cytoplasmic translocation is regulated by mechanical signaling, protein modification, and metabolism. Cell Biol Int 44:1416–1425
19. Totaro A, Panciera T, Piccolo S (2018) YAP/TAZ upstream signals and downstream responses. Nat Cell Biol 20:888–899
20. Kim J, Kim YH, Kim J et al (2017) YAP/TAZ regulates sprouting angiogenesis and vascular barrier maturation. J Clin Invest 127:3441–3461
21. Sakabe M, Fan J, Odaka Y et al (2017) YAP/TAZ-CDC42 signaling regulates vascular tip cell migration. Proc Natl Acad Sci U S A 114:10918–10923
22. Koo JH, Guan KL (2018) Interplay between YAP/TAZ and metabolism. Cell Metab 28:196–206
23. Zhang X, Zhao H, Li Y et al (2018) The role of YAP/TAZ activity in cancer metabolic reprogramming. Mol Cancer 17:134
24. Wang W, Xiao ZD, Li X et al (2015) AMPK modulates Hippo pathway activity to regulate energy homeostasis. Nat Cell Biol 17:490–499
25. Song L, Tang H, Liao W et al (2017) FOXC2 positively regulates YAP signaling and promotes the glycolysis of nasopharyngeal carcinoma. Exp Cell Res 357:17–24
26. Feng Y, Wang J, Yuan Y et al (2018) miR-539-5p inhibits experimental choroidal neovascularization by targeting CXCR7. FASEB J 32:1626–1639
27. Feng YF, Guo H, Yuan F (2015) Lipopolysaccharide promotes choroidal neovascularization by up-regulation of CXCR4 and CXCR7 expression in choroid endothelial cell. PLoS ONE 10:e136175
28. Chen J, Li F, Xu Y et al (2019) Cholesterol modification of SDF-1-specific siRNA enables therapeutic targeting of angiogenesis through Akt pathway inhibition. Exp Eye Res 184:64–71
29. Soutschek J, Akinc A, Bramlage B et al (2004) Therapeutic silencing of an endogenous gene by systemic administration of modified siRNAs. Nature 432:173–178
30. Lambert V, Lecomte J, Hansen S et al (2013) Laser-induced choroidal neovascularization model to study age-related macular degeneration in mice. Nat Protoc 8:2197–2211
31. Connor KM, Krah NM, Dennison RJ et al (2009) Quantification of oxygen-induced retinopathy in the mouse: a model of vessel loss, vessel regrowth and pathological angiogenesis. Nat Protoc 4:1565–1573
32. Baker M, Robinson SD, Lechertier T et al (2011) Use of the mouse aortic ring assay to study angiogenesis. Nat Protoc 7:89–104
33. Mammoto T, Muyleart M, Mammoto A (2019) Endothelial YAP1 in regenerative lung growth through the angiopoietin-Tie2 pathway. Am J Respir Cell Mol Biol 60:117–127
34. Mammoto A, Muyleart M, Kadlec A et al (2018) YAP1-TEAD1 signaling controls angiogenesis and mitochondrial biogenesis through PGC1alpha. Microvasc Res 119:73–83
35. Witmer AN, Vrensen GF, Van Noorden CJ et al (2003) Vascular endothelial growth factors and angiogenesis in eye disease. Prog Retin Eye Res 22:1–29
36. Jin J, Yuan F, Shen MQ et al (2013) Vascular endothelial growth factor regulates primate choroid-retinal endothelial cell proliferation and tube formation through PI3K/Akt and MEK/ERK dependent signaling. Mol Cell Biochem 381:267–272
37. Takata K, Morishige K, Takahashi T et al (2008) Fasudil-induced hypoxia-inducible factor-1alpha degradation disrupts a hypoxia-driven vascular endothelial growth factor autocrine mechanism in endothelial cells. Mol Cancer Ther 7:1551–1561
38. Nilsson I, Shibuya M, Wennstrom S (2004) Differential activation of vascular genes by hypoxia in primary endothelial cells. Exp Cell Res 299:476–485
39. Wang X, Freire VA, Schermann G et al (2017) YAP/TAZ orchestrate VEGF signaling during developmental angiogenesis. Dev Cell 42:462–478
40. Aouiss A, Anka ID, Kabine M et al (2019) Update of inflammatory proliferative retinopathy: Ischemia, hypoxia and angiogenesis. Curr Res Transl Med 67:62–71
41. Grunwald JE, Metelitsina TI, Dupont JC et al (2005) Reduced foveolar choroidal blood flow in eyes with increasing AMD severity. Invest Ophthalmol Vis Sci 46:1033–1038
42. Makin RD, Apicella I, Nagasaka Y et al (2018) RF/6A chorioretinal cells do not display key endothelial phenotypes. Invest Ophthalmol Vis Sci 59:5795–5802
43. Rezzola S, Belleri M, Gariano G et al (2014) In vitro and ex vivo retina angiogenesis assays. Angiogenesis 17:429–442
44. Choi HJ, Zhang H, Park H et al (2015) Yes-associated protein regulates endothelial cell contact-mediated expression of angiopoietin-2. Nat Commun 6:6943
45. Zhu M, Liu X, Wang Y et al (2018) YAP via interacting with STAT3 regulates VEGF-induced angiogenesis in human retinal microvascular endothelial cells. Exp Cell Res 373:155–163
46. Yan Z, Shi H, Zhu R et al (2018) Inhibition of YAP ameliorates choroidal neovascularization via inhibiting endothelial cell proliferation. Mol Vis 24:83–93
47. Yu P, Wilhelm K, Dubrac A et al (2017) FGF-dependent metabolic control of vascular development. Nature 545:224–228
48. Obach M, Navarro-Sabate A, Caro J et al (2004) 6-Phosphofructo-2-kinase (pfkfb3) gene promoter contains hypoxia-inducible factor-1 binding sites necessary for transactivation in response to hypoxia. J Biol Chem 279:53562–53570
49. Fukasawa M, Tsuchiya T, Takayama E et al (2004) Identification and characterization of the hypoxia-responsive element of the human placental 6-phosphofructo-2-kinase/fructose-2,6-bisphosphatase gene. J Biochem 136:273–277
50. Zhu B, Pan S, Liu J et al (2020) HIF-1alpha forms regulatory loop with YAP to coordinate hypoxia-induced adriamycin resistance in acute myeloid leukemia cells. Cell Biol Int 44:456–466
51. Jia Y, Li HY, Wang J et al (2019) Phosphorylation of 14-3-3zeta links YAP transcriptional activation to hypoxic glycolysis for tumorigenesis. Oncogenesis 8:31
52. Zhang X, Li Y, Ma Y et al (2018) Yes-associated protein (YAP) binds to HIF-1alpha and sustains HIF-1alpha protein stability to promote hepatocellular carcinoma cell glycolysis under hypoxic stress. J Exp Clin Cancer Res 37:216
53. Xu J, Li Y, Hong J (2014) Progress of anti-vascular endothelial growth factor therapy for ocular neovascular disease: benefits and challenges. Chin Med J (Engl) 127:1550–1557

54. Andreoli CM, Miller JW (2007) Anti-vascular endothelial growth factor therapy for ocular neovascular disease. Curr Opin Ophthalmol 18:502–508
55. Penn JS, Madan A, Caldwell RB et al (2008) Vascular endothelial growth factor in eye disease. Prog Retin Eye Res 27:331–371
56. Aiello LP, Northrup JM, Keyt BA et al (1995) Hypoxic regulation of vascular endothelial growth factor in retinal cells. Arch Ophthalmol 113:1538–1544
57. Hunt TK, Aslam RS, Beckert S et al (2007) Aerobically derived lactate stimulates revascularization and tissue repair via redox mechanisms. Antioxid Redox Signal 9:1115–1124

Publisher's Note Springer Nature remains neutral with regard to jurisdictional claims in published maps and institutional affiliations.